Time-Dependent Upwelling in the Tropical Lower Stratosphere Estimated from the Zonal-Mean Momentum Budget

WILLIAM J. RANDEL, ROLANDO R. GARCIA, AND FEI WU

National Center for Atmospheric Research, Boulder, Colorado*

(Manuscript received 12 April 2001, in final form 20 December 2001)

ABSTRACT

Dynamical variability in the extratropical stratosphere occurs on a broad range of timescales, from daily to seasonal. Extratropical wave transience is correlated with variations in the mean meridional (Brewer–Dobson) circulation that links the Tropics and the extratropics. In this study, the variability of observed temperature and calculated vertical velocity in the tropical lower stratosphere is examined to isolate the imprint of forcing by extratropical waves. The influence of the waves is quantified by estimating zonal-mean tropical upwelling from the zonal-mean momentum balance on a daily basis; a large fraction of the variance of tropical upwelling occurs at periods of 10–40 days, forced by transient waves. In addition, significant coherence is found between calculated upwelling and observed temperatures in the tropical lower stratosphere on weekly to seasonal timescales. This relationship is quantitatively consistent with simple thermodynamic balance, and suggests that the large annual cycle of temperature near the tropical tropopause is mainly a result of the relatively long radiative timescales in that region. The results indicate that EP flux divergence due to extratropical waves is a major determinant of zonal-mean temperatures in the tropical lower stratosphere.

1. Introduction

The existence of a strong annual cycle in the zonal-mean temperature of the tropical lower stratosphere, together with the absence of a similar seasonal variation in the troposphere, suggests that the large-scale stratospheric circulation exerts a strong influence on the tropical lower stratosphere (Yulaeva et al. 1994; Holton et al. 1995; Reid and Gage 1996). The global mean meridional circulation, which links the Tropics and extratropics, is driven by the seasonal cycle of radiative heating, plus forcing due to the dissipation of vertically propagating Rossby and gravity waves (Garcia 1987; Holton 1990; Dunkerton 1991; Haynes et al. 1991; Iwasaki 1992; Plumb and Eluszkiewicz 1999). Model calculations and observations indicate that the maximum in extratropical wave forcing occurs during September–November in the Southern Hemisphere, and during November–March in the Northern Hemisphere, so that the global forcing has a seasonal maximum centered on Northern Hemisphere winter. This produces a seasonal cycle in the Brewer–Dobson circulation that is reflected in the seasonal cycle of temperature in the tropical lower stratosphere (Reed and Vlcek 1969; Yulaeva et al. 1994). However, higher-frequency transience in tropical upwelling, and its coupling to tropical temperature, has received relatively little attention.

The extratropical waves that drive the stratospheric circulation often occur in episodes or bursts of wave activity emanating from the troposphere. Typically four to six such events occur each winter, each one lasting 1–2 weeks. Their episodic nature is illustrated by the time series of the vertical component of EP flux F_z at 100 mb for the year July 1994–June 1995, shown in Fig. 1. The solid line in the figure denotes horizontally averaged F_z in the Northern Hemisphere extratropics (40°–70°N), and the dashed line shows the same quantity in the Southern Hemisphere (40°–70°S). As noted above, the global forcing has a relative maximum during September–March, due to the combined effects of the fluxes from both hemispheres. This particular year is interesting because many of the Northern Hemisphere wave events are clearly separated in time, allowing their global influence to be identified.

Time series of zonal mean temperature in the Tropics (averaged over 10°N–10°S) are also shown in Fig. 1 at three levels spanning the upper troposphere to lower stratosphere. Superimposed on the large annual cycle in the time series at 68 and 100 mb are periods of episodic cooling and warming that appear to be cor-

* The National Center for Atmospheric Research is sponsored by the National Science Foundation.

Corresponding author address: Dr. William J. Randel, National Center for Atmospheric Research, P.O. Box 3000, Boulder, CO 80307-3000.
E-mail: randel@ncar.edu

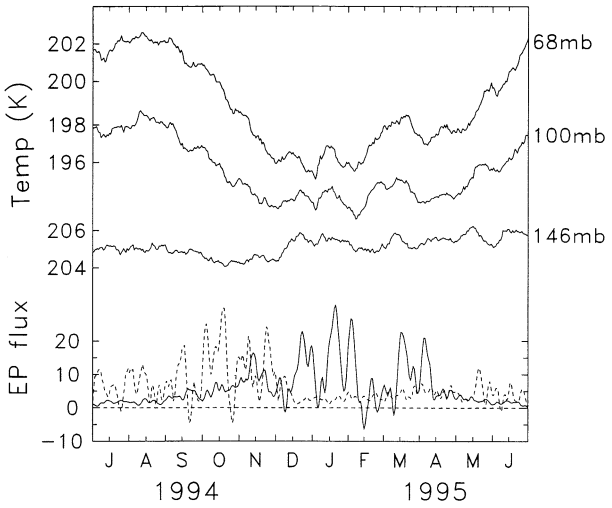

FIG. 1. Bottom curves show time series of extratropical 100-mb eddy heat flux during 1994–1995 for the Northern Hemisphere (solid line, 40°–70°N) and for the Southern Hemisphere (dashed line, 40°–70°S). The eddy heat flux is proportional to the vertical component of the EP flux, and is used to quantify the amount of wave activity entering the extratropical stratosphere. The upper curves show contemporaneous time series of zonal-mean temperatures in the Tropics (10°N–10°S), for the 68-, 100-, and 146-mb levels. Note several transient cooling episodes at 68 and 100 mb, which are correlated with extratropical wave events.

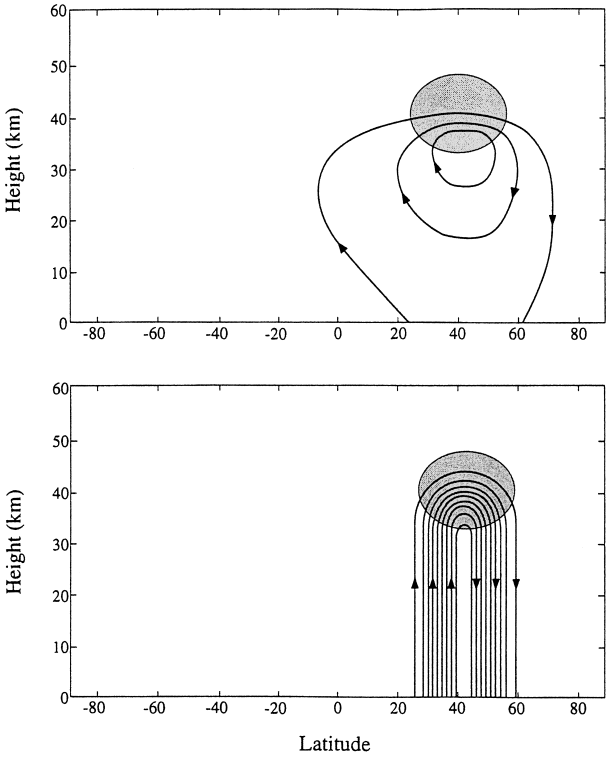

FIG. 2. The mean meridional streamfunction induced by periodic EP flux divergence of frequency σ applied within the shaded region in an atmosphere with radiative relaxation timescale α^{-1}. The upper panel shows the quasi-adiabatic response ($\sigma/\alpha \gg 1$); the lower panel illustrates the quasi-steady-state ($\sigma/\alpha \ll 1$), downward control situation. Adapted from Holton et al. (1995).

related with midlatitude planetary wave events (with cold temperatures often following maxima in wave activity). The cooling events are less evident at the 146-mb level (below the tropopause), which also exhibits small seasonality in comparison with higher altitudes. The planetary wave events are also associated with high-latitude warming (not shown); such out-of-phase polar–tropical temperature anomalies are clear evidence of global-scale circulation effects (as noted in the first satellite observations of these events by Fritz and Soules 1970). Similar transient, out-of-phase latitudinal variations are observed in satellite ozone measurements (Randel 1993; Fusco and Salby 1999). We note that periods of reduced wave forcing in Fig. 1 (such as the second half of February 1995) are associated with warming of the tropical lower stratosphere, probably due to relaxation towards radiative equilibrium. This is consistent with calculations showing that the the zonal mean temperature in the region near and above the tropical tropopause is below radiative equilibrium (Olaguer et al. 1992); this departure from equilibrium is maintained by the stratospheric circulation (Thuburn and Craig 1997, 2000).

The presence of coherent transient signals in both Tropics and extratropics, such as seen in Fig. 1, suggests that they may be useful for quantifying the influence of the extratropics on the tropical lower stratosphere. The Tropics and extratropics are linked through the mean meridional (Brewer–Dobson) circulation, with upwelling occurring in the Tropics. The goal of this study is to quantify the variability of tropical upwelling and its relationship to forcing by extratropical waves, on both seasonal and subseasonal timescales. In section 2, we use the zonal-mean momentum budget to obtain an expression for upwelling averaged over the Tropics and applicable over all timescales. The tropical mean upwelling estimated in this fashion is compared with results obtained from the thermodynamic budget, for both seasonal variability (section 3) and higher-frequency transience (section 4). We also derive, in section 5, a simple relationship between upwelling and zonal-mean temperatures averaged over the Tropics and use it to ascertain whether our estimates of upwelling from the momentum budget are consistent with the behavior of tropical temperatures. These comparisons reveal generally good agreement and suggest that extratropical wave forcing is an important determinant of tropical temperatures in the lower stratosphere. Our results are summarized, and their implications discussed, in section 6.

2. Data and analyses

a. Met Office data and Eliassen–Palm flux divergence

The data used in this study are daily stratospheric meteorological analyses from the Met Office (UKMO) stratosphere–troposphere assimilation (Swinbank and

O'Neill 1994). These data are available from October 1991 to the present, with a 2.5° × 2.5° latitude–longitude grid and ~2.5 km vertical grid length (output on standard pressure levels, with six levels per decade of pressure). For our analyses we calculate the daily zonally averaged temperature and zonal winds, together with the zonal mean eddy fluxes of heat $\overline{v'T'}$ and momentum $\overline{u'v'}$. These are, in turn, used to calculate the scaled Eliassen–Palm (EP) flux divergence

$$\mathrm{DF} = \frac{\exp(z/H)}{a\cos\phi}\nabla\cdot\mathbf{F}, \tag{1}$$

where **F** is the EP flux vector, whose components are

$$F_\phi = \exp(-z/H)a\cos\phi\left[-\overline{u'v'} + \left(\frac{\partial\overline{u}}{\partial z}\right)\left(\frac{\overline{v'T'}}{S}\right)\right], \tag{2a}$$

$$F_z = \exp(-z/H)a\cos\phi\left[\hat{f}\frac{\overline{v'T'}}{S}\right], \quad \text{and} \tag{2b}$$

$$\hat{f} = f - \frac{1}{a\cos\phi}\frac{\partial}{\partial\phi}(\overline{u}\cos\phi). \tag{3}$$

The notation used here follows Andrews et al. (1987). The vertical coordinate is $z = H\ln(p_0/p)$ with $p_0 =$ 1000 mb and $H = 7$ km; f is the Coriolis parameter, a is the radius of the earth, and ϕ is the latitude. Overbars denote zonal means and primes are deviations therefrom. Here, S is the static stability parameter, equal to HN^2/R; N^2 is the Brunt–Vaisala frequency; and R is the gas constant, 287 $m^2\ s^{-2}\ K^{-1}$. Note that these calculations do not include a contribution to F_z associated with vertical eddy fluxes $\overline{u'w'}$. These fluxes would be due primarily to gravity waves, which are not resolved in UKMO analyses.

b. Tropical upwelling from thermodynamic balance

A common method of estimating the mean meridional circulation ($\overline{v}^*$, $\overline{w}^*$) is based on the quasigeostrophic transformed Eulerian mean (TEM) thermodynamic and continuity equations:

$$\frac{\partial\overline{T}}{\partial t} + \overline{v}^*\frac{1}{a}\frac{\partial\overline{T}}{\partial\phi} + \overline{w}^*S = \overline{Q}, \tag{4}$$

$$\frac{1}{a\cos\phi}\frac{\partial}{\partial\phi}(\overline{v}^*\cos\phi) + e^{z/H}\frac{\partial}{\partial z}(\overline{w}^*e^{-z/H}) = 0, \tag{5}$$

where $\overline{Q}$ is the zonal mean radiative heating rate (see Solomon et al. 1986; Gille et al. 1987; Rosenlof 1995; Eluszkiewicz et al. 1996). The quasigeostrophic approximation used here neglects an eddy forcing term in the thermodynamic equation that can be shown to be small, particularly in the Tropics (Gille et al. 1987; Eluszkiewicz et al. 1996). We derive daily estimates of $\overline{Q}$ using the radiative code of Olaguer et al. (1992), with input of daily UKMO temperatures and climatological values of ozone, water vapor, and other radiatively active constituents. The thermodynamic and continuity equations are solved iteratively to obtain global estimates of ($\overline{v}^*$, $\overline{w}^*$). We will denote the vertical velocity derived by this method by $\overline{w}^*_Q$, because it is primarily derived from radiative heating calculations.

An important point concerning the calculation of $\overline{w}^*_Q$ is that its global average on pressure surfaces should be zero, but this is usually not achieved due to uncertainties in the calculation of radiative heating rates (especially in the lower stratosphere, where the net values are small). Since there is no a priori method of enforcing this constraint, we simply add a latitude-independent correction factor to $\overline{w}^*_Q$ in order to force its global integral to vanish. This correction is of order 0.05 mm s^{-1}, or about 15% of typical values of $\overline{w}^*_Q$ in the Tropics. One effect of enforcing this constraint on daily calculations of $\overline{w}^*_Q$ is that the magnitude of transient fluctuations in the Tropics is reduced (by about 40% at 100 mb). The sensitivity of the variance of $\overline{w}^*_Q$ to the (arbitrary) zero global mean constraint should be borne in mind in the detailed discussions of $\overline{w}^*_Q$ to follow.

The solution of Eqs. (4)–(5) yields the mean vertical velocity as a function of latitude and height. We then define a tropical average vertical velocity as

$$\langle\overline{w}^*_Q\rangle(z) = \frac{\displaystyle\int_{-\phi_0}^{\phi_0}\overline{w}^*_Q(\phi, z)a\cos\phi\, d\phi}{\displaystyle\int_{-\phi_0}^{\phi_0}a\cos\phi\, d\phi}, \tag{6}$$

where the angle brackets denote latitudinal averaging, and the range of integration $\pm\phi_0$ defines the tropical region. We define a tropical average vertical velocity because, as shown below, momentum balance cannot be used to estimate the vertical velocity as a function of latitude in the deep Tropics; instead, the momentum equation yields an estimate of the vertical velocity averaged over a range of tropical latitudes, which can be compared to the results of Eq. (6).

c. Tropical upwelling from momentum balance

An estimate of the mean vertical velocity integrated across the Tropics can also be obtained from the TEM momentum equation

$$\frac{\partial\overline{u}}{\partial t} - \hat{f}\overline{v}^* + \overline{w}^*\frac{\partial\overline{u}}{\partial z} = \mathrm{DF}, \tag{7}$$

where DF and $\hat{f}$ are given by (1) and (3). The continuity equation (5) implies that the TEM meridional circulation ($\overline{v}^*$, $\overline{w}^*$) can be obtained from a streamfunction $\overline{\chi}^*$, such that

$$(\overline{v}^*, \overline{w}^*) = \frac{1}{e^{-z/H}\cos\phi}\left(-\frac{\partial\overline{\chi}^*}{\partial z}, \frac{1}{a}\frac{\partial\overline{\chi}^*}{\partial\phi}\right). \tag{8}$$

Combining (7) and (8), it is straightforward to show that

$$\overline{\chi}^*(\phi, z) = -\frac{\cos\phi}{\hat{f}} \int_z^\infty [\mathrm{DF}(\phi, z') - \overline{u}_t(\phi, z')]_{\overline{m}} e^{-z'/H}\, dz', \tag{9}$$

where $\overline{m} = a\cos\phi(\overline{u} + a\Omega\cos\phi)$ is the zonal mean angular momentum, Ω is the angular rotation frequency of the earth, and the integral (9) is evaluated along contours of constant $\overline{m}(\phi, z)$ (Haynes et al. 1991).

From (8) and (9), it follows that

$$\overline{w}_m^*(\phi, z) = \frac{1}{e^{-z/H}\cos\phi}\frac{1}{a}\frac{\partial}{\partial\phi}\{\overline{\chi}^*(\phi, z)\} = \frac{e^{z/H}}{\cos\phi}\frac{1}{a}\frac{\partial}{\partial\phi}\left\{-\frac{\cos\phi}{\hat{f}}\int_z^\infty [\mathrm{DF}(\phi, z') - \overline{u}_t(\phi, z')]_{\overline{m}} e^{-z'/H}\, dz'\right\}, \tag{10}$$

where the notation $\overline{w}_m^*$ is meant to denote the fact that the mean vertical velocity (10) is obtained from the momentum budget. Equation (10) cannot be used to estimate $\overline{w}_m^*$ in the deep Tropics, where $\hat{f}$ tends to vanish. However, the equation can be integrated with respect to latitude to yield the tropical average vertical velocity

$$\begin{aligned}\langle\overline{w}_m^*\rangle(z) &= \frac{e^{z/H}}{\displaystyle\int_{-\phi_0}^{\phi_0} a\cos\phi\, d\phi}[\overline{\chi}^*(\phi_0, z) - \overline{\chi}^*(-\phi_0, z)] \\ &= \frac{e^{z/H}}{\displaystyle\int_{-\phi_0}^{\phi_0} a\cos\phi\, d\phi}\left\{\frac{-\cos\phi}{\hat{f}(z, \phi)}\int_z^\infty [\mathrm{DF}(\phi, z') - \overline{u}_1(\phi, z')]_{\overline{m}} e^{-z'/H}\, dz'\right\}_{-\phi_0}^{+\phi_0},\end{aligned} \tag{11}$$

where the range $\pm\phi_0$ again defines the tropical region, the only restriction being that these latitudes must be chosen sufficiently far from the equator that $\hat{f}$ is not too small. Another practical constraint is that obtaining observational estimates of DF also becomes problematic in the Tropics. In practice, (11) yields reasonable results for $\pm\phi_0 \geq 20°$.

We note that, while (11) provides an estimate of the vertical velocity averaged over the latitude range $\pm\phi_0$, it says nothing about how $\overline{w}_m^*$ is distributed in latitude over the Tropics. Implicit in some of the analyses to follow is the assumption that $\overline{w}_m^*$ is more or less uniformly distributed, even on seasonal timescales, consistent with behavior derived from the thermodynamic budget (see Fig. 3 below).

Under steady-state conditions, Eq. (10) reduces to the familiar ''downward control principle'' (Haynes et al. 1991). Without the steady-state restriction, Eqs. (10) and (11) include a contribution from $\overline{u}_t$ that can arise in various ways. At low frequencies, changes in $\overline{u}$ are most likely associated with the seasonal cycle of diabatic heating; at higher frequencies, $\overline{u}_t$ may be due to transient heating fluctuations and also to the influence of transient EP flux divergence, either locally or remotely. To illustrate the last point, Fig. 2 shows the mean meridional circulation produced by steady-state and transient wave forcing. The steady-state case, shown in the lower panel of the figure, is the familiar downward control situation, wherein (in the absence of friction) the meridional circulation is limited to the range of latitudes where the EP flux divergence is nonzero. The upper panel of the figure shows that, under transient conditions, the wave-induced meridional circulation extends well outside the forcing region; in this case, the Coriolis torque acting on the circulation away from the forcing can induce changes in the mean zonal wind $\overline{u}$.

d. Spectral analyses

Some of the results presented in this paper are based on cross-spectrum analyses between daily time series of tropical vertical velocities and temperatures. Spectra for the eight individual years, 1992–99, are obtained from direct Fourier analyses, following standard formulas (Jenkins and Watts 1968); the results are then averaged to give a composite spectrum. The composite spectrum is smoothed with a five-point running mean, yielding 80 ($8 \times 5 \times 2$) degrees of freedom (since the spectral estimates for each year have 2 degrees of freedom). The approximate 95% and 99% significance levels for the coherence-squared (coh^2) statistic are 0.08 and 0.11, respectively. The 95% confidence limits for the phase spectra are determined following Jenkins and Watts (1968, section 9.2).

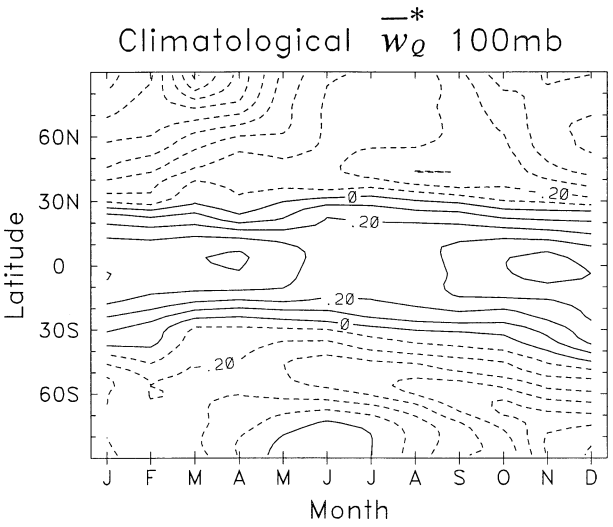

FIG. 3. Climatological vertical velocity at 100 mb derived from thermodynamic balance $\overline{w}^*_Q$, based on UKMO temperatures for 1992–99. The contour interval is 0.1 mm s^{-1}.

3. Seasonal variation of tropical upwelling

We examine first the seasonal cycle of tropical upwelling, comparing estimates from the thermodynamic and momentum balance calculations, Eqs. (6) and (11), respectively. All results are based on monthly means for the period 1992–99. For reference, Fig. 3 shows the mean vertical velocity $\overline{w}^*_Q$ at 100 mb calculated from the thermodynamic equation as a function of month and latitude (i.e., without averaging over the Tropics). Tropical upwelling has a minimum during Northern Hemisphere summer and a broad maximum in winter. The magnitudes obtained here (maxima of $\sim$0.40 mm s^{-1} and minima of $\sim$0.25 mm s^{-1}) are in reasonable agreement with the results of Eluszkiewicz et al. (1996), which were derived from different input fields and independent radiative balance calculations. Our results at 68 mb (not shown) reveal a larger-amplitude seasonal cycle, with values in good agreement with the results obtained by Rosenlof (1995) for 70 mb.

The 100-mb $\overline{w}^*_Q$ in Fig. 3 shows a slight latitudinal movement of the tropical upwelling region, with the ''turnaround latitude'' (where $\overline{w}^*_Q = 0$) shifted toward the Southern Hemisphere during December–February. A more substantial latitudinal shift is found at higher altitudes (not shown). This seasonal variation of the turnaround latitude implies that there is no single range of latitudes that encompasses the entire upwelling region throughout the year; below we compare results using different latitude limits in Eqs. (6) and (11).

The climatological latitudinal structure of the streamfunction $\overline{\chi}^*$, derived from momentum balance per Eq. (9), is shown in Fig. 4 for the months of December, March, June, and September. These plots include the total streamfunction, and also the separate contributions from wave forcing DF and zonal wind tendency $\overline{u}_t$. The

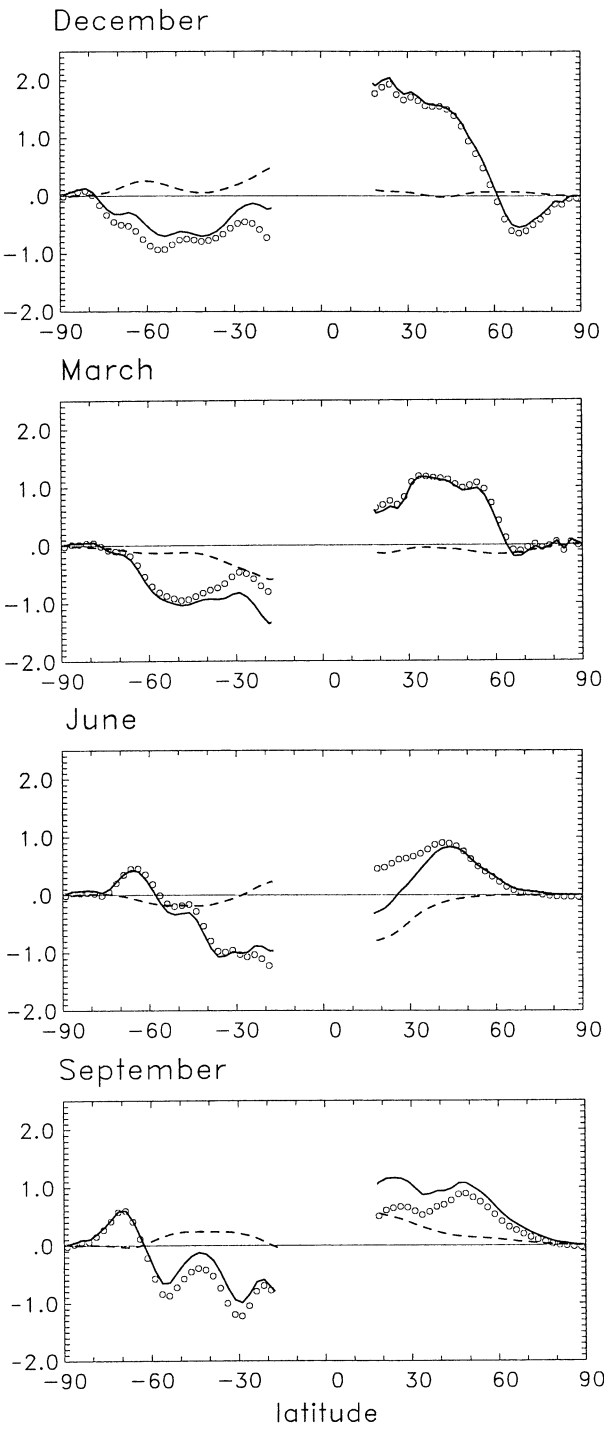

FIG. 4. Latitudinal structure of terms in the 100-mb TEM streamfunction $\overline{\chi}^*$ derived from momentum balance, Eq. (9), based on climatology for 1992–99. Shown are monthly results for Dec, Mar, Jun, and Sep. The solid lines denote the total streamfunction, and the circles and dashed lines indicate the separate contributions from the DF and $\overline{u}_t$ terms.

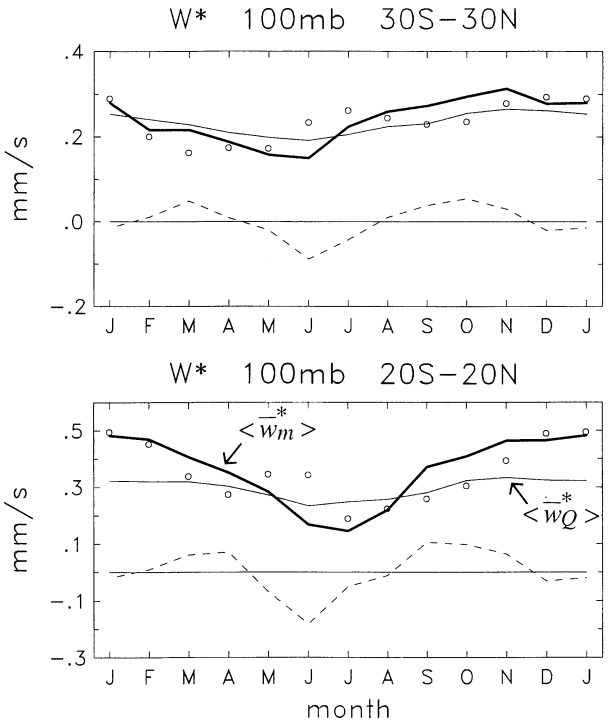

FIG. 5. Climatological seasonal variation of tropical upwelling at 100 mb derived from thermodynamic balance $\langle \overline{w}^*_Q \rangle$ (light solid line) and momentum balance $\langle \overline{w}^*_m \rangle$ (heavy solid line). Upwelling is averaged over $\pm 30°$ (top) and $\pm 20°$ (bottom). The individual contributions from DF (circles) and $\overline{u}_t$ (dashed line) to the momentum balance calculation are also indicated.

latter is generally small, but can ocassionally become important, especially in Northern Hemisphere summer.

Figure 5 compares the seasonal cycle in tropical upwelling at 100 mb calculated by the thermodynamic and momentum methods, comparing results for averages over $\pm 30°$ and $\pm 20°$ [$\langle \overline{w}^*_Q \rangle$ is area-averaged over these latitudes per Eq. (6), while $\langle \overline{w}^*_m \rangle$ is evaluated from Eq. (11) using the appropriate latitude limits]. The figure also displays the separate contributions to $\langle \overline{w}^*_m \rangle$ from DF and $\overline{u}_t$. For both latitude limits the annual mean values and the phase of the seasonal cycle of $\langle \overline{w}^*_Q \rangle$ and $\langle \overline{w}^*_m \rangle$ are in good agreement. However, the amplitude of the seasonal cycle is substantially larger in $\langle \overline{w}^*_m \rangle$ than in $\langle \overline{w}^*_Q \rangle$ for the results averaged over $\pm 20°$.

The agreement in the estimates of tropical upwelling averaged over $\pm 30°$ is encouraging, given that they are obtained by completely different methods. The differences in upwelling estimates averaged over $\pm 20°$ (in particular, the much larger seasonal cycle in $\langle \overline{w}^*_m \rangle$) could reflect uncertainties in either calculation. According to Rosenlof (1995), uncertainties in the tropical radiative heating rates correspond to substantial uncertainties in $\overline{w}^*_Q$ (of order $\pm 50\%$), although analyses of short-lived tropical constituents suggest smaller uncertainties (better than $\pm 30\%$; Flocke et al. 1999). The seasonal cycle in tropical vertical velocity derived from water vapor observations (Mote et al. 1996; Andrews et al. 1999) is similar to that of $\overline{w}^*_Q$ in Fig. 1, but its amplitude is not tightly constrained by such calculations. As for the estimates of $\langle \overline{w}^*_m \rangle$, they are sensitive to the EP flux divergence calculations at low latitudes, which are uncertain at best, and in any case do not include the effects of unresolved scales (gravity waves). Rosenlof and Holton's (1993) work suggests that, at least in the National Center for Atmospheric Research (NCAR) Community Climate Model (CCM2), parameterized gravity wave drag can make an important contribution to $\langle \overline{w}^*_m \rangle$. Thus, it is possible that the neglect of gravity wave effects could account in part for the differences in the estimates of $\langle \overline{w}^*_m \rangle$ and $\langle \overline{w}^*_Q \rangle$ shown in Fig. 5.

Figures 4 and 5 also show that the term $\overline{u}_t$ in Eq. (11) contributes significantly to the seasonal variation of tropical upwelling. In particular, the seasonal minimum during June–July is strongly influenced by $\overline{u}_t$. The behavior of $\overline{u}_t$ appears to be due primarily to the Northern Hemisphere summer monsoon circulation, which is associated with a marked transition from zonal mean westerlies in Northern Hemisphere subtropics to summer easterlies. The resulting $\overline{u}_t$ patterns maximize in Northern Hemisphere low latitudes during June and September. A similar but smaller amplitude variation is observed in low latitudes of the Southern Hemisphere during December and March, and this also influences the details of the seasonality of tropical upwelling. Overall, the seasonal variation of $\overline{u}_t$ gives rise to a marked semiannual contribution to $\langle \overline{w}^*_m \rangle$, as can be appreciated from Fig. 5.

Note, however, that the annual average of $\overline{u}_t$ must be zero. This implies that the annual mean $\langle \overline{w}^*_m \rangle$ estimated from Eq. (11) is due solely to DF at the boundaries $\pm \phi_0$ of the tropical region (Plumb and Eluszkiewicz 1999), unless $\overline{u}_t$ correlates with the factor $\hat{f}$ in the denominator of (11) in such a way as to produce a nonzero annual average. Figure 5 indicates that this is not the case, since the contribution of that part of $\langle \overline{w}^*_m \rangle$ due to $\overline{u}_t$ has nearly zero annual mean.

4. Subseasonal variability

Time series of $\langle \overline{w}^*_Q \rangle$ and $\langle \overline{w}^*_m \rangle$ at 100 mb are shown in Fig. 6 for the year July 1994 to June 1995, based on averages over $\pm 30°$. These daily results indicate a high degree of variability in tropical upwelling over a broad range of weekly to monthly timescales. There is reasonably good agreement between $\langle \overline{w}^*_Q \rangle$ and $\langle \overline{w}^*_m \rangle$, with a statistically significant correlation of 0.55, although the transients are somewhat larger in the $\langle \overline{w}^*_m \rangle$ results. Figure 6 covers the same period as Fig. 1, and comparison of the two figures shows that many of the individual peaks in tropical upwelling occur in concert with maxima in extratropical wave activity (the peaks in the lower curves in Fig. 1). Note that this correspondence cannot be expected to be exact, since upwelling responds to the vertical integral of EP flux divergence at $\pm \phi_0$, per Eq. (1), whereas Fig. 1 shows

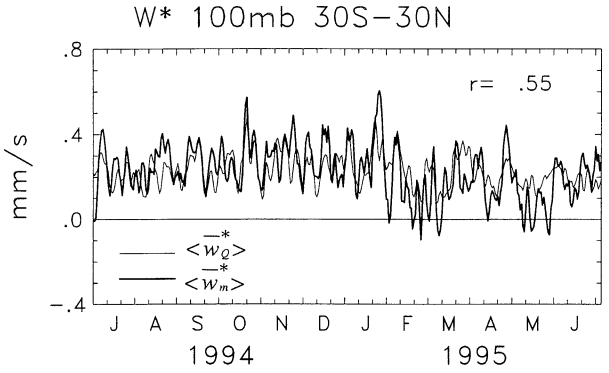

FIG. 6. Time series of 100-mb vertical velocity averaged over ±30° during 1994–95, evaluated from the thermodynamic (light line) and momentum (heavy line) budgets. The temporal correlation is 0.55.

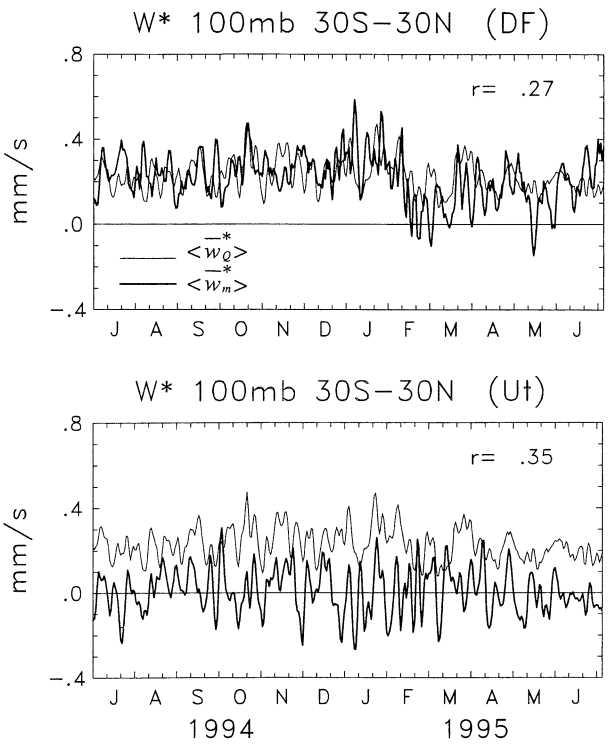

FIG. 7. Time series of the the contributions to the tropical zonal-mean vertical velocity evaluated from the momentum budget (heavy lines) due to (top) DF and (bottom) $\overline{u}_t$. Also shown in both panels is the zonal-mean vertical velocity calculated from the thermodynamic budget.

only the vertical component of EP flux at 100 mb averaged over 40°–70°; even so, the correlation between the two time series is 0.40.

It is interesting to examine the relative contributions of DF and $\overline{u}_t$ to $\langle \overline{w}^*_m \rangle$ on subseasonal timescales. Figure 7 shows daily correlations of $\langle \overline{w}^*_Q \rangle$ with that part of $\langle \overline{w}^*_m \rangle$ due to each of these terms. Comparison with Fig. 6 reveals that the individual contributions to $\langle \overline{w}^*_m \rangle$ are much less well correlated with $\langle \overline{w}^*_Q \rangle$ than their sum ($r = 0.27$ and 0.35 versus $r = 0.55$). Furthermore, the two contributions are not particularly well correlated with each other either ($r = -0.36$, not shown), suggesting that a significant portion of the zonal wind tendency must be the result of Coriolis torques operating on the meridional circulation forced by remote wave dissipation, as illustrated by the top panel of Fig. 2. We emphasize again that, although $\overline{u}_t$ makes an important contribution to transient $\langle \overline{w}^*_m \rangle$, the annual average of this contribution vanishes, leaving DF as the only source of annual mean tropical upwelling.

Although not directly relevant to the Tropics, Fig. 8 shows comparisons of $\langle \overline{w}^*_Q \rangle$ and $\langle \overline{w}^*_m \rangle$ evaluated over Northern Hemisphere midlatitudes (30°–60°N) and polar regions (60°–90°N). These independent estimates of vertical velocity are in good agreement in both regions and show a high degree of variability, similar to that seen in the Tropics. One notable difference between $\langle \overline{w}^*_m \rangle$ and $\langle \overline{w}^*_Q \rangle$ is seen in the polar region: while the temporal correlations are quite high ($r = 0.70$), $\langle \overline{w}^*_m \rangle$ systematically underestimates wintertime maxima compared to $\langle \overline{w}^*_Q \rangle$. The result is that the winter–spring seasonal maximum in polar downwelling seen in Fig. 3 is not well captured in the $\langle \overline{w}^*_m \rangle$ estimates. This may be due to problems estimating the EP flux divergence in polar regions from operational analyses. Another possibility is that unresolved gravity waves may be providing additional forcing of the meridional circulation at these latitudes. Calculations in the Southern Hemisphere (not shown) reveal very similar results to those in Fig. 7 (including systematic underestimates in $\langle \overline{w}^*_m \rangle$ compared to $\langle \overline{w}^*_Q \rangle$ in the polar region).

Returning to tropical variability, Fig. 9 shows power- and cross-spectrum analyses between $\langle \overline{w}^*_m \rangle$ and $\langle \overline{w}^*_Q \rangle$ averaged over ±30°, evaluated from daily calculations over the period 1992–1999. The power spectra (Fig. 9a) show broad maxima in each quantity at periods between about 10–40 days, in addition to the large maxima at the annual period. The power estimates from $\langle \overline{w}^*_m \rangle$ are approximately a factor of 2–2.5 larger than those from $\langle \overline{w}^*_Q \rangle$, indicating that peak-to-peak variations in $\langle \overline{w}^*_m \rangle$ are about 1.5 times larger (consistent with the time series shown in Fig. 6). However, as noted earlier, the magnitude of transient fluctuations in $\langle \overline{w}^*_Q \rangle$ is sensitive to the method used to enforce the zero global mean constraint on $\overline{w}^*_Q$. If the constraint is not applied, the variability of $\langle \overline{w}^*_Q \rangle$ is larger by about 40% (although still somewhat smaller than the variability of $\langle \overline{w}^*_m \rangle$).

The cross-spectral calculations show highly significant coherence between $\langle \overline{w}^*_m \rangle$ and $\langle \overline{w}^*_Q \rangle$ over a wide range of periods (Fig. 9b), with variability ocurring nearly in phase (Fig. 9c). There is a slight phase difference (~30°) at the lowest frequencies (seasonal cycle), which can also be appreciated in the seasonal cycles shown in Fig. 5. However, the amplitude of the seasonal cycle is relatively small, especially for $\langle \overline{w}^*_Q \rangle$. Furthermore, estimates of $\langle \overline{w}^*_m \rangle$ from different meteorological datasets [e.g., National Centers for Environmental Prediction (NCEP)–NCAR reanalyses or European Centre

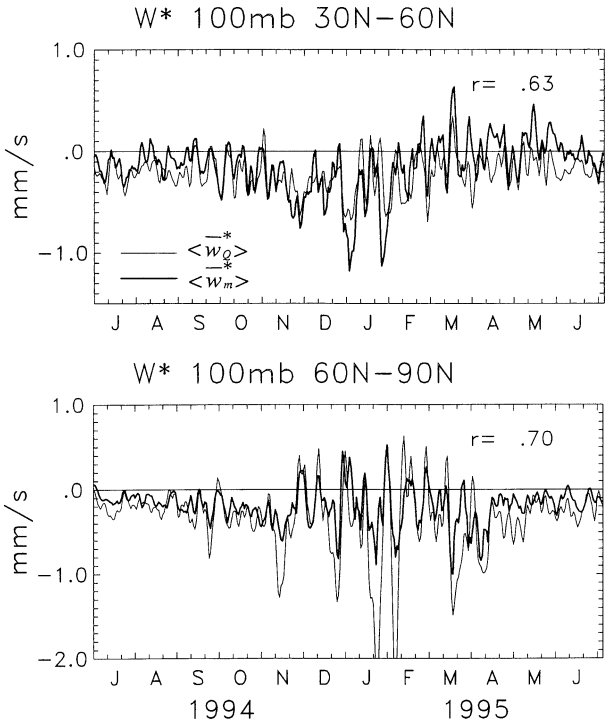

FIG. 8. As in Fig. 6, but for the Northern Hemisphere extratropics. Results are shown for averages over 30°–60°N (top) and 60°–90°N (bottom).

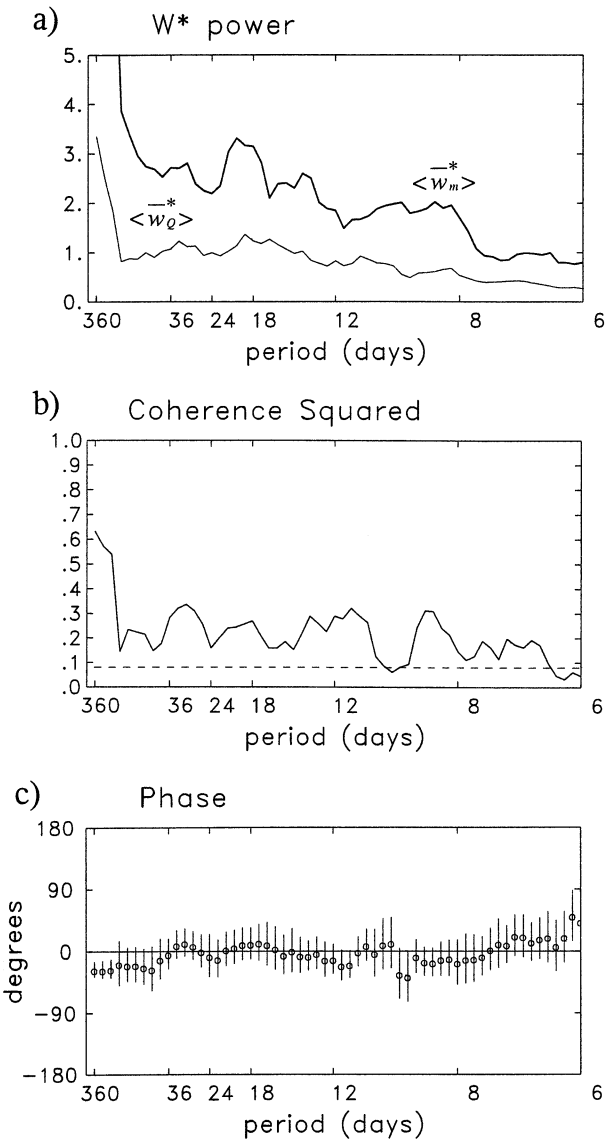

FIG. 9. (a) Power spectra at 100 mb of $\langle \overline{w}^*_Q \rangle$ (light line) and $\langle \overline{w}^*_m \rangle$ (dark line) evaluated over ±30° from daily data for 1992–99. Units are 10^{-4} mm^2 s^{-2}, and spectra are shown only for periods longer than 6 days. (b) Coherence squared and (c) phase spectra between $\langle \overline{w}^*_Q \rangle$ and $\langle \overline{w}^*_m \rangle$. The 95% confidence limits of both statistics are indicated.

for Medium-Range Weather Forecasts (ECMWF) analyses] give slightly different annual cycles due to variations in the estimates of DF, so that the annual phase of $\langle \overline{w}^*_m \rangle$ is uncertain to within ±30°. Overall, the variability in tropical upwelling estimated from the momentum budget is in reasonably good agreement with thermodynamic estimates over a broad range of weekly to seasonal timescales, with somewhat larger transient variability in the results from the momentum budget.

5. Relationship between tropical upwelling and temperature

The foregoing results show that $\langle \overline{w}^*_m \rangle$ agrees rather well with $\langle \overline{w}^*_Q \rangle$ over a broad range of timescales, and suggest that the former is a valid estimate of tropical upwelling. The influence of extratropical wave forcing on the Tropics is now quantified by examining the relationship between the vertical velocity calculated from momentum balance $\langle \overline{w}^*_m \rangle$ and the observed zonal mean temperature averaged over the Tropics $\langle \overline{T} \rangle$. A correlation can be seen by inspection of the time series of $\langle \overline{w}^*_m \rangle$ (Fig. 6) and tropical temperature (Fig. 1). For example, the large wave event in late January 1995, is associated with zonal mean tropical cooling of ~2 K at 68 and 100 mb. A more systematic examination can by made by means of a cross-spectral analysis of $\langle \overline{w}^*_m \rangle$ and $\langle \overline{T} \rangle$, using data for the years 1992–99.

The relationship between $\langle \overline{w}^*_m \rangle$ and $\langle \overline{T} \rangle$ can be interpreted in terms of the following simplified version of the thermodynamic equation (4):

$$\frac{\partial \overline{T}}{\partial t} + \overline{w}^* S = -\alpha(\overline{T} - \overline{T}_e), \tag{12}$$

where the mean horizontal advection term has been neglected and heating is parameterized as a simple relaxation to the radiative equilibrium temperature $\overline{T}_e$ with an inverse radiative timescale α^{-1}. In the Tropics, $\overline{T}_e$ does not have a strong seasonal variation and may be considered constant in time. Then, assuming harmonic expansions of the form

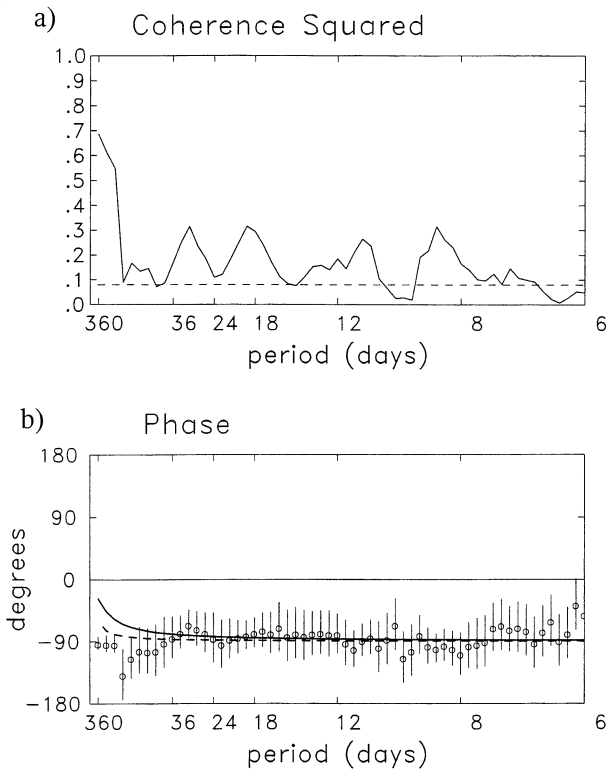

FIG. 10. Coherence squared and phase spectra between extratropically forced 100-mb vertical velocity $\langle \overline{w}^*_m \rangle$ (averaged over $\pm 30°$) and 100-mb zonal-mean temperature $\langle \overline{T} \rangle$ averaged over $\pm 30°$, calculated from daily data for 1992–99. The 95% confidence limits are shown for both quantities. The solid and dashed lines in (b) are the phase relations expected from thermodynamic balance, Eq. (14), using $\alpha = 1/30$ day^{-1} and 1/100 day^{-1}, respectively.

$$[\overline{T}(t), \overline{w}^*(t)] = \sum [T_\sigma, w_\sigma] \exp(i\sigma t), \qquad (13)$$

where σ represents frequency, gives the following relationship between frequency components of $\overline{T}$ and $\overline{w}^*$:

$$T_\sigma = -w_\sigma S \frac{\alpha - i\sigma}{\alpha^2 + \sigma^2}. \qquad (14)$$

At high frequencies ($\sigma \gg \alpha$), $T_\sigma \rightarrow -w_\sigma[(S/\sigma)] \exp(-i\pi/2)$; that is, T_σ and w_σ are in quadrature (with temperature minima following velocity maxima as a result of adiabatic cooling). The low end of the frequency range is limited by the annual cycle $\sigma = 2\pi/365 \approx 1/58$ day^{-1}. This is comparable to the inverse radiative timescale in the lower stratosphere, which has been estimated to be between 1/30 day^{-1} (Newman and Rosenfield 1997; Hartmann et al. 2001, hereafter HHF) and 1/100 day^{-1} (Kiehl and Solomon 1986; Mlynczak et al. 1999). Using these values in Eq. (14) yields $T_\sigma \approx -w_\sigma[S/(2.18\sigma)] \exp(-i\ 27.5°)$ for $\alpha = 1/30$ day^{-1}, and $T_\sigma \approx -w_\sigma[S/(1.16\sigma)] \exp(-i\ 59.8°)$ for $\alpha = 1/100$ day^{-1}.

Figure 10 shows coh^2 and phase spectra at 100 mb between $\langle \overline{w}^*_m \rangle$ and $\langle \overline{T} \rangle$ (averaged over $\pm 30°$). The coh^2 values are statistically significant at most periods in the range between 10 days and 1 yr, and they are particularly large at seasonal timescales. The phase spectrum is shown in Fig. 10b, together with solid and dashed lines that indicate the phase relationships expected from Eq. (14), using radiative timescale of $\alpha = 1/30$ day^{-1} and 1/100 day^{-1}, respectively. The observed and calculated phases show good agreement at most periods, but there is some departure from the theoretical estimates at the lowest (seasonal to annual) periods. The difference is considerably smaller when α is set to 1/100 day^{-1} in Eq. (14), suggesting that this value of the radiative timescale is more consistent with the observed seasonal cycle of temperature in the tropical lower stratosphere in the context of the present calculations. We return to this point below.

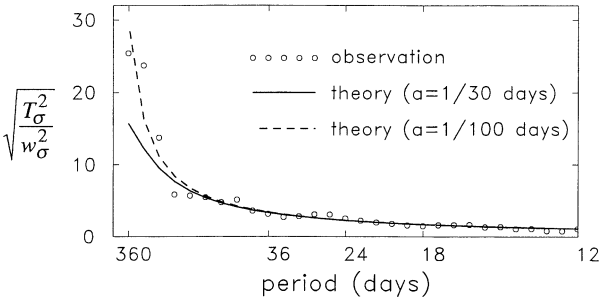

FIG. 11. The circles show the ratio $R_\sigma = \sqrt{T_\sigma^2/w_\sigma^2}$ (K mm^{-1} s) of tropical temperature variance to tropical upwelling variance (computed from momentum balance) at 100 mb. The solid and dashed lines show the ratio expected from thermodynamic balance, Eq. (16), using radiative damping rates of $\alpha = 1/30$ day^{-1} and 1/100 day^{-1}, respectively.

The relative magnitude of temperature and vertical velocity variations can be quantified in terms of the ratio of power spectral estimates for each time series:

$$R_\sigma = \sqrt{\frac{T_\sigma^2}{w_\sigma^2}}. \qquad (15)$$

This gives an estimate of the temperature sensitivity to variations in vertical velocity at each frequency, and these can be directly compared with estimates derived from Eq. (14); that is,

$$R_\sigma = \frac{S}{\sqrt{\alpha^2 + \sigma^2}}. \qquad (16)$$

Figure 11 compares "observed" R_σ (computed using UKMO temperatures and vertical velocities obtained from our momentum budget calculations) against theoretical values predicted by (16) for $\alpha = 1/30$ day^{-1} and 1/100 day^{-1}. Here, R_σ shows greatly enhanced temperature response at low frequency, with remarkably good agreement between the observed and theoretical ratios. At the lowest frequencies, the data are most consistent with the theoretical curve for $\alpha = 1/100$ day^{-1}; at high frequencies, the valued of α is irrelevant, as implied by Eq. (16). Values of R_σ computed using

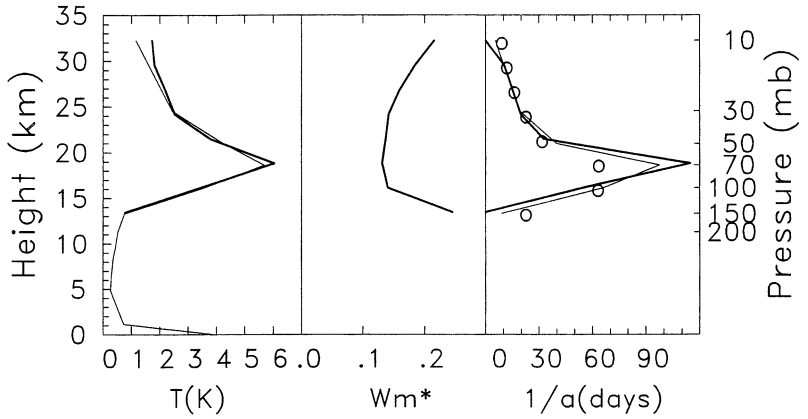

FIG. 12. (left) Amplitude of the annual harmonic of tropical mean temperature $\langle\overline{T}\rangle$ derived from UKMO data (heavy line) and NCEP reanalysis (light line). (center) Amplitude of annual harmonic of $\langle\overline{w}_m\rangle$ averaged over $\pm 30°$ (mm s^{-1}). (right) vertical profile of the radiative relaxation timescale $\tau = \alpha^{-1}$ (days) derived from the profiles of $\langle\overline{T}\rangle$ and $\langle\overline{w}_m\rangle$ using Eq. (17); results are shown for both UKMO (heavy line) and NCEP (light line) estimates of $\langle\overline{T}\rangle$. The circles denote estimates of τ from longwave heating calculations per Eq. (19). See text for details.

$\langle\overline{w}^*_Q\rangle$ (not shown) are larger at most frequencies than those obtained from $\langle\overline{w}^*_m\rangle$, and they do not fit the theoretical curve as closely. This is related to the larger transient variability of $\langle\overline{w}^*_m\rangle$ compared to $\langle\overline{w}^*_Q\rangle$ (Figs. 6 and 9a), and the sensitivity of the latter to the zero global mean constraint.

The enhanced sensitivity of tropical temperature to upwelling velocity at low frequencies predicted by Eq. (16) and shown in Fig. 11 may help explain the large amplitude of the seasonal temperature cycle in the tropical lower stratosphere seen in Fig. 1, the precise value being ultimately determined by magnitude of the radiative relaxation timescale. Thus, small α (long radiative timescale) will result in a large seasonal cycle of temperature, and vice versa. To test this idea, one can solve Eqs. (15)–(16) for $\tau = \alpha^{-1}$:

$$\tau = \frac{1}{\sqrt{\left(\frac{w_\sigma}{T_\sigma}\right)^2 S^2 - \sigma^2}}, \tag{17}$$

which can then be evaluated at $\sigma = 2\pi/365$ day^{-1}, using estimates of w_σ obtained from the momentum balance calculations.

Figure 12 shows vertical profiles of the amplitude of the annual component of $\langle\overline{T}\rangle$ and $\langle\overline{w}^*_m\rangle$, together with the the radiative relaxation timescale calculated from Eq. (17) using these annual cycle profiles.[1] The annual component of $\langle\overline{T}\rangle$ has a pronounced maximum in the lower stratosphere, peaking at 68 mb, whereas the annual component of $\langle\overline{w}^*_m\rangle$ is nearly constant between about 100 and 30 mb. The corresponding profile of τ then maximizes in the lower stratosphere, which is generally consistent with previous calculations of τ, except that it peaks at 68 mb rather than at 100 mb as is the case with most estimates of τ obtained directly from longwave heating rate calculations (e.g., Kiehl and Solomon 1986; Mlynczak et al. 1999). Note that similar results are obtained regardless of whether UKMO or NCEP reanalysis data are used in the calculations; this is a consequence of the rather good agreement between the UKMO and NCEP temperature data. Nevertheless, small differences in the annual cycle of $\langle\overline{T}\rangle$ in the lower stratosphere (6.0 K in UKMO data versus 5.6 K in NCEP data at 68 mb) can lead to more substantial differences in the estimates of τ (115 versus 95 days).

We have also calculated the radiative relaxation timescale by performing a spectral analysis of the equation

$$\overline{Q} = -\alpha(\overline{T} - \overline{T}_e), \tag{18}$$

where $\overline{Q}$ is the heating rate calculated with the code of Olaguer et al. (1992), and $\overline{T}$ is the observed temperature. An estimate of the relaxation time $\tau = \alpha^{-1}$ then follows from

$$\tau = \sqrt{\frac{T^2_\sigma}{Q^2_\sigma}}, \tag{19}$$

where, as before, σ denotes frequency. This procedure is analogous to that used in conventional estimates of τ, which are obtained from the longwave heating rates computed for slighly different temperature profiles: in Eq. (19), the variances of $\overline{Q}$ and $\overline{T}$ play the role of perturbations of the reference heating rate and temperature profile. The results of evaluating Eq. (19) for the annual cycle ($\sigma = 2\pi/365$ day^{-1}) are denoted by the circles in the right-hand panel of Fig. 12. Overall, the resulting profile of τ agrees quite well with the com-

[1] The results depend also on the value of S, which is proportional to N^2. In the calculations we have used profiles of N^2 derived from UKMO observations of annual mean temperature in the Tropics.

pletely independent estimate obtained from Eq. (17) except at 68 mb, where Eq. (17) yields somewhat larger values.

The point that emerges clearly from Fig. 12 is that the observed annual cycle of $\langle\overline{T}\rangle$ and the calculated annual cycle of $\langle\overline{w}^*_m\rangle$ in the tropical lower stratosphere are consistent with large values of τ in the region between 46 and 100 mb (about 16–22 km). Conversely, it may be said that the observed large annual cycle of $\langle\overline{T}\rangle$ at these levels arises from the slow radiative relaxation timescale coupled with a near constant annual cycle in upwelling.

6. Summary and discussion

Variability in extratropical planetary waves produces transience in the mean meridional (Brewer–Dobson) circulation which couples the tropical and extratropical stratosphere. Transient events are observed in temperatures throughout the tropical stratosphere, extending downward to near the tropopause (~100 mb), providing evidence for the influence on the Tropics of extratropical wave forcing. In this study we have attempted to quantify the coupling between the tropical temperatures, vertical velocities, and extratropical wave forcing over a wide range of timescales.

The seasonal cycle of tropical vertical velocity $\langle\overline{w}^*_m\rangle$ calculated from the momentum balance is slightly larger than that computed from the thermodynamic balance $\langle\overline{w}^*_Q\rangle$ (Fig. 5). At higher frequencies, $\langle\overline{w}^*_m\rangle$ also shows reasonably good agreement with $\langle\overline{w}^*_Q\rangle$ (Fig. 6), although transients in the former are approximately 1.5 times larger than in the latter. Both calculations indicate that a large fraction of the variance in tropical upwelling occurs at periods of ~10–40 days; thus, entry of air into the tropical stratosphere may occur episodically, rather than in a slow uplift modulated only by the seasonal cycle.

The estimates of tropical upwelling from the momentum budget presented here are not, in general, downward control calculations. Equation (11) gives the tropical average of the zonal-mean upwelling in terms of the Eliassen–Palm flux divergence DF and the tendency of the zonal mean wind $\overline{u}_t$ evaluated at the latitudinal boundaries of the tropical region. The inclusion of $\overline{u}_t$ allows variability in the zonal wind to influence the estimates of $\langle\overline{w}^*_m\rangle$. As argued in section 2, such variability likely arises from the seasonal cycle in $\overline{u}$ at low frequencies, and from local or remote transients in DF at higher frequencies. However, the annual mean $\langle\overline{w}^*_m\rangle$ due to $\overline{u}_t$ vanishes, as shown in Figs. 5 and 7, so annual mean tropical upwelling is driven solely by the time average of DF at the boundaries of the tropical region (cf. Plumb and Eluszkiewicz 1999).

Discrepancies between our estimates of $\langle\overline{w}^*_m\rangle$ and $\langle\overline{w}^*_Q\rangle$ may be due to a variety of causes. The detailed radiative calculations needed to compute $\langle\overline{w}^*_Q\rangle$ are suspect in the tropical lower stratosphere (due to the small net value of the heating rate there), and require adjustment to ensure global continuity. Furthermore, the calculations presented here do not take into account the radiative effects of any cirrus clouds near the tropical tropopause (HHF). The momentum balance calculations needed to compute $\langle\overline{w}^*_m\rangle$ are sensitive to EP flux divergence estimates in the subtropics, which are also of questionable quality in the lower stratosphere. In addition, the EP fluxes resolved in UKMO data neglect any contribution from unresolved scales (gravity waves). Given these uncertainties, the overall agreement between $\langle\overline{w}^*_Q\rangle$ and $\langle\overline{w}^*_m\rangle$ found here is encouraging. At present there are no strong observational constraints from other data sources (such as trace constituents) to provide independent estimates of transience in tropical vertical velocity in the lower stratosphere.

A further implication of this work is that much of the observed variability in zonal-mean tropical temperature may be quantitatively explained in terms of the tropical upwelling $\langle\overline{w}^*_m\rangle$ estimated from the momentum budget. This is demonstrated by significant coherence between observed tropical temperatures and $\langle\overline{w}^*_m\rangle$. Furthermore, the observed phase difference and relative amplitude of tropical temperature $\langle\overline{T}\rangle$ and $\langle\overline{w}^*_m\rangle$ are quantitatively consistent with simple thermodynamic balance considerations. For realistic values of the radiative time in the lower stratosphere, the phase difference and relative amplitude are relatively constant over a wide range of transient timescales (shorter than ~60 days). However, the response of $\langle\overline{T}\rangle$ to $\langle\overline{w}^*_m\rangle$ is greatly enhanced (by approximately one order of magnitude) at seasonal timescales. Thus, the vertical profile of the radiative damping timescale (large in the lowest stratosphere) may help explain the large annual cycle of temperature observed in this region.

Acknowledgments. This work was partially supported by NASA Grants W-18181 and W-162-15, under the ACMAP and UARS Guest Investigator programs. J.-F. Lamarque and B.A. Boville provided constructive reviews. We are also grateful to Dr. Alan Plumb and two anonymous reviewers for their comments on the original manuscript. The National Center for Atmospheric Research is operated by the University Corporation for Atmospheric Research.

REFERENCES

Andrews, A. E., K. A. Boering, B. C. Daube, S. C. Wofsy, E. J. Hintsa, E. M. Weinstock, and T. P. Bui, 1999: Empirical age spectra for the lower tropical stratosphere from in situ observations of CO_2: Implications for stratospheric transport. *J. Geophys. Res.*, **104,** 26 581–26 595.

Andrews, D. G., J. R. Holton, and C. B. Leovy, 1987: *Middle Atmosphere Dynamics.* Academic Press, 489 pp.

Dunkerton, T. J., 1991: Nonlinear propagation of zonal winds in an atmosphere with Newtonian cooling and equatorial wavedriving. *J. Atmos. Sci.*, **48,** 236–263.

Eluszkiewicz, J., and Coauthors, 1996: Residual circulation in the

stratosphere and lower mesosphere as diagnosed from Microwave Limb Sounder data. *J. Atmos. Sci.,* **53,** 217–240.

Flocke, F., and Coauthors, 1999: An examination of chemistry and transport processes in the tropical lower stratosphere using observations of long-lived and short-lived compounds obtained during STRAT and POLARIS. *J. Geophys. Res.,* **104,** 26 625–26 642.

Fritz, S., and S. D. Soules, 1970: Large-scale temperature changes in the stratosphere observed from *Nimbus III. J. Atmos. Sci.,* **27,** 1091–1097.

Fusco, A., and M. L. Salby, 1999: Interannual variations of total ozone and their relationship to variations of planetary wave activity. *J. Climate,* **12,** 1619–1629.

Garcia, R. R., 1987: On the mean meridional circulation of the middle atmosphere. *J. Atmos. Sci.,* **44,** 3599–3609.

Gille, J. C., L. V. Lyjak, and A. K. Smith, 1987: The global residual mean circulation in the middle atmosphere for the northern winter period. *J. Atmos. Sci.,* **44,** 1437–1452.

Hartmann, D. L., J. R. Holton, and Q. Fu, 2001: The heat balance of the tropical tropopause, cirrus, and stratospheric dehydration. *Geophys. Res. Lett.,* **28,** 1969–1972.

Haynes, P. H., C. J. Marks, M. E. McIntyre, T. G. Shepherd, and K. P. Shine, 1991: On the ''downward control'' of extratropical diabatic circulations by eddy-induced mean zonal forces. *J. Atmos. Sci.,* **48,** 651–678.

Holton, J. R., 1990: On the global exchange of mass between the stratosphere and troposphere. *J. Atmos. Sci.,* **47,** 392–395.

——, P. Haynes, M. McIntyre, A. Douglass, R. Rood, and L. Pfister, 1995: Stratosphere–troposphere exchange. *Rev. Geophys.,* **33,** 403–439.

Iwasaki, T., 1992: General circulation diagnosis in the pressure-isentrope hybrid vertical coordinate. *J. Meteor. Soc. Japan,* **70,** 673–686.

Jenkins, G. M., and D. G. Watts, 1968: *Spectral Analysis and Its Applications.* Holden-Day, 525 pp.

Kiehl, J. T., and S. Solomon, 1986: On the radiative balance of the stratosphere. *J. Atmos. Sci.,* **43,** 1525–1534.

Mlynczak, M. G., C. J. Mertens, R. R. Garcia, and R. W. Portmann, 1999: A detailed evaluation of the stratospheric heat budget. 2. Global radiation balance and diabatic circulations. *J. Geophys. Res.,* **104,** 6039–6066.

Mote, P. W., and Coauthors, 1996: An atmospheric tape recorder: The imprint of tropical tropopause temperatures on stratospheric water vapor. *J. Geophys. Res.,* **101,** 3989–4006.

Newman, P. A., and J. E. Rosenfield, 1997: Stratospheric thermal damping times. *Geophys. Res. Lett.,* **24,** 433–436.

Olaguer, E. P., H. Yang, and K. K. Tung, 1992: A reexamination of the radiative balance of the stratosphere. *J. Atmos. Sci.,* **49,** 1242–1263.

Plumb, R. A., and J. Eluszkiewicz, 1999: The Brewer–Dobson circulation: Dynamics of the tropical upwelling. *J. Atmos. Sci.,* **56,** 868–890.

Randel, W. J., 1993: Global variations of zonal mean ozone during stratospheric warming events. *J. Atmos. Sci.,* **50,** 3308–3321.

Reed, R. J., and C. L. Vlcek, 1969: The annual temperature variation in the lower tropical stratosphere. *J. Atmos. Sci.,* **26,** 163–167.

Reid, G., and K. Gage, 1996: The tropical tropopause over the western Pacific: Wave driving, convection and the annual cycle. *J. Geophys. Res.,* **101,** 21 233–21 241.

Rosenlof, K. H., 1995: Seasonal cycle of the residual mean meridional circulation in the stratosphere. *J. Geophys. Res.,* **100,** 5173–5191.

——, and J. R. Holton, 1993: Estimates of the stratospheric residual circulation using the downward control principle. *J. Geophys. Res.,* **98,** 10 465–10 479.

Solomon, S., J. T. Kiehl, R. R. Garcia, and W. Grose, 1986: Tracer transport by the diabatic circulation deduced from satellite observations. *J. Atmos. Sci.,* **43,** 1603–1617.

Swinbank, R., and A. O'Neill, 1994: A stratosphere–troposphere data assimilation system. *Mon. Wea. Rev.,* **122,** 686–702.

Thuburn, J., and G. C. Craig, 1997: GCM tests of theories for the height of the tropopause. *J. Atmos. Sci.,* **54,** 869–882.

——, and ——, 2000: Stratospheric influence on tropopause height: The radiative constraint. *J. Atmos. Sci.,* **57,** 17–28.

Yulaeva, E., J. R. Holton, and J. M. Wallace, 1994: On the cause of the annual cycle in tropical lower-stratospheric temperatures. *J. Atmos. Sci.,* **51,** 169–174.